Title

Antitumor Immune Responses in B2M-Deficient Cancers.

Journal

Cancer Immunology Research, 11(12)

ISSN

2326-6066

Authors

Torrejon, Davis Y
Galvez, Mildred
Abril-Rodriguez, Gabriel
et al.

Publication Date

2023-12-01

DOI

10.1158/2326-6066.cir-23-0139

Peer reviewed

HHS Public Access

Author manuscript

Cancer Immunol Res. Author manuscript; available in PMC 2024 June 01.

Published in final edited form as:

Cancer Immunol Res. 2023 December 01; 11(12): 1642–1655. doi:10.1158/2326-6066.CIR-23-0139.

Antitumor Immune Responses in *B2M*-Deficient Cancers

Davis Y. Torrejon[1,*], **Mildred Galvez**[2,*], **Gabriel Abril-Rodriguez**[1,2], **Katie M. Campbell**[1], **Egmidio Medina**[1], **Agustin Vega-Crespo**[1], **Anusha Kalbasi**[3], **Begoña Comin-Anduix**[4,5], **Antoni Ribas**[1,2,4,5,6]

[1.]Department of Medicine, Division of Hematology-Oncology, University of California, Los Angeles (UCLA)

[2.]Department of Molecular and Medical Pharmacology, UCLA

[3.]Department of Radiation Oncology, UCLA

[4.]Department of Surgery, Division of Surgical Oncology, UCLA

[5.]Jonsson Comprehensive Cancer Center, Los Angeles, CA 90095, USA

[6.]Parker Institute for Cancer Immunotherapy, San Francisco, CA 94129, USA

Abstract

β2-microglobulin (B2M) is a critical component of the MHC class I molecule and is required to present tumor antigens to T cells. Its loss results in acquired resistance to immune checkpoint blockade (ICB) therapies. However, there have been well-documented cases of *B2M*-inactivated tumors responding to ICB, justifying investigation of how an antitumor immune response can be generated to tumors without surface MHC class I. We knocked-out *B2M* in three murine models with varying baseline MHC class I expression and sensitivity to anti-programmed death receptor (PD-1) therapy and analyzed the immune responses. MC38 and YUMMER2.1 without *B2M* responded to anti–PD-1 alone or with an IL2 agonist, and this was mediated by $CD4^+$ T cells and natural killer (NK) cells. The more aggressive B16 without *B2M* expression only partially responded to the IL2 agonist, and this was dependent on NK cells. When analyzing nearly 300 pretreatment biopsies from patients with melanoma receiving PD-1 blockade–based therapies, we

Correspondence: Antoni Ribas, M.D., Ph.D., Department of Medicine, Division of Hematology-Oncology, 650 Charles E. Young Dr South, 54-100A CHS, Los Angeles, CA, 90095-1782, USA. Telephone: 210-206-3928. Fax: 310-825-2493. aribas@mednet.ucla.edu.
*Equal contribution as first authors

Author disclosures: D.Y.T. is currently a full-time employee of Ascendis Pharma. K.M.C. has received consulting fees from PACT Pharma, Tango Therapeutics, and Geneoscopy LLC, and is a shareholder in Geneoscopy LLC. G.A-R. has received honoraria from consulting with Arcus Biosciences. A.R. has received honoraria from consulting with Amgen, Bristol-Myers Squibb, Chugai, Jazz, Merck, Novartis, RAPT, is or has been a member of the scientific advisory board and holds stock in Advaxis, Appia, Apricity, Arcus, Compugen, CytomX, Highlight, ImaginAb, ImmPact, ImmuneSensor, Inspirna, Isoplexis, Kite-Gilead, Larkspur, Lutris, MapKure, Merus, PACT, Pluto, RAPT, Synthekine and Tango, has received research funding from Agilent and from Bristol-Myers Squibb through Stand Up to Cancer (SU2C), and patent royalties from Arsenal Bio.

Conflict of Interest Statement

D.Y.T. is currently a full-time employee of Ascendis Pharma. K.M.C. has received consulting fees from PACT Pharma, Tango Therapeutics, and Geneoscopy LLC, and is a shareholder in Geneoscopy LLC. G.A-R. has received honoraria from consulting with Arcus Biosciences. A.R. has received honoraria from consulting with Amgen, Bristol-Myers Squibb, Chugai, Jazz, Merck, Novartis, RAPT, is or has been a member of the scientific advisory board and holds stock in Advaxis, Appia, Apricity, Arcus, Compugen, CytomX, Highlight, ImaginAb, ImmPact, ImmuneSensor, Inspirna, Isoplexis, Kite-Gilead, Larkspur, Lutris, MapKure, Merus, PACT, Pluto, RAPT, Synthekine and Tango, has received research funding from Agilent and from Bristol-Myers Squibb through Stand Up to Cancer (SU2C), and patent royalties from Arsenal Bio.

found infrequent *B2M* mutations or homozygous loss but more frequent loss of heterozygosity (LOH) or copy number gains. *B2M* LOH was enriched in biopsies from patients without response to therapy, and these biopsies were more frequently infiltrated by activated NK cells. We conclude that in the absence of *B2M,* activation of $CD4^+$ T cells and NK cells can mediate responses to murine models of PD-1 blockade therapy. Additionally, in human melanoma the intratumoral presence of activated NK cells upon partial *B2M* loss likely selects against tumor escape through low surface MHC class I expression.

Keywords

Immune checkpoint blockade; PD-1; B2M; Melanoma; HLA

Introduction

The success of immune checkpoint blockade (ICB) therapies relies on the antitumor activity of $CD8^+$ T cells (1,2). However, $CD8^+$ T cell–based therapies rely on functional antigen presentation by tumor cells, which opens avenues for the development of resistance mechanisms. Canonically, tumor antigens are presented to $CD8^+$ T cells by surface MHC class I molecules, which are composed of a heavy chain and β−2-microglobulin (B2M). B2M is necessary for the proper stabilization and folding of MHC class I molecules. In its absence, the MHC class I complex does not reach the cell surface and is degraded (3). The loss of MHC class I through *B2M* mutations or copy number losses results in the inability of $CD8^+$ T cells to recognize cancer cells and has long been recognized to lead to tumor immunotherapy resistance (4–8). However, the use of ICB in highly immunogenic cancers that may have already gone through immune editing has demonstrated that some patients whose cancers do not express *B2M* can still respond to anti–PD-1 therapies (9–15). Therefore, there is a need to study how the immune system can induce responses in *B2M*-null tumors by analyzing murine models and studying patient-derived biopsies. Previously, we reported that anti–PD-1 resistance due to *B2M* loss could be overcome with the activation of natural killer (NK) cells and $CD4^+$ T cells in murine models (16). The role of $CD4^+$ T cells in immune responses to *B2M*-knockout (KO) tumors has been corroborated in murine models and biopsy samples of patients with DNA mismatch repair deficient (MMR-d) cancers (13). Furthermore, γδ T cells have also been shown to increase in MMR-d cancers with *B2M* defects, and to have a cytotoxic effect upon treatment with ICB (15). Nevertheless, the exact effect of defects in MHC class I antigen presentation machinery on anti–PD-1 therapy response, and the cells capable of mediating the antitumorigenic effects of PD-1 blockade in *B2M*-defective human tumors, have not been fully characterized.

Here we used CRISPR/Cas9 to develop sublines through *B2M*-KO mutations in three murine tumor models: MC38 and YUMMER2.1, which have high immunogenicity due to carcinogen-induced high mutational load and have $CD4^+$ and $CD8^+$ T-cell co-dependency in response to anti–PD-1 therapy, and the lowly immunogenic B16 model with undetectable baseline MHC class I expression and primary $CD8^+$ T-cell dependency to respond to immunotherapy (17). These murine models allowed us to study the mechanisms by which immune cells orchestrate responses to PD-1 blockade in the context of *B2M* inactivation.

To further corroborate these findings, we analyzed sequencing data from a large cohort of pretreatment biopsies from patients with melanoma for the presence of *B2M* somatic alterations and correlative infiltrating immune cell subsets. Our findings may support the development of combination strategies to potentiate the $CD8^+$ T-cell antitumor effects and avoid resistance to ICB therapies.

Materials and Methods

Mice, cell lines and reagents

All mouse studies were approved by the UCLA Animal Research Committee under protocol #2004-159-43I. Female C57BL/6N mice were obtained from the UCLA Department of Radiation Oncology Animal Core. Mice were bred and kept under defined flora and pathogen-free conditions at the Association for the Assessment and Accreditation of Laboratory Animal Care (AAALAC) approved animal facility of the Division of Experimental Radiation Oncology, UCLA. The MC38 mouse colon adenocarcinoma cell line was initially generated at the NCI Surgery Branch (originally Colo38) and was obtained from Dr. Robert Prins, UCLA Department of Neurosurgery (2014). The B16-F10 mouse melanoma cell line was purchased from ATCC (Manassas, VA, Cat #CRL-6475, 2017). The YUMM2.1 UV mouse melanoma cell line was obtained from Dr. Marcus Bosenberg, Yale University (2009). The MC38, B16-F10, and YUMM2.1 UV mouse cell lines and subsequently established knockout cell lines (see *CRISPR/Cas9-mediated gene knockout*) were cultured at 37º C and 5% CO_2 in Dulbecco's Modified Eagle Medium (DMEM) (Corning, Manassas, VA, Cat #MT10013CM) supplemented with 10% FBS (Omega, Tarzana, CA, Cat #FB-21), 100 units/ml penicillin, 100 μg/ml streptomycin, and 0.25 μg/ml amphotericin B (Omega, Cat #AA-40). Cell lines were tested for mycoplasma contamination using the MycoAlert Mycoplasma Detection Kit (Lonza, Walkersville, MD, Cat #LT07-218), and were regularly tested for authentication. For *in vivo* experiments, early passage cell lines (no more than ten passages) were utilized.

Antibodies for *in vivo* experiments were as follows: anti-mouse PD-1 (clone RMP1-14 Cat #BE0146), anti-mouse CD8 (clone YTS 169.4, BE0117 Cat #BE0117), anti-mouse CD4 (clone GK1.5, BE0003 Cat #BE0003), anti-mouse NK1.1 (clone PK136, BE0036 Cat #BE0036), anti-mouse CD40L (clone MR-1, BP0017 Cat #BP0017), anti-mouse IFNγ (clone XMG1.2, BE0055 Cat #BE0055) and isotype control antibody (clone 2A3, BE0089 Cat #BE0089), all from BioXCell (West Lebanon, NH). Bempegaldesleukin (NKTR-214) (20) was provided by Nektar Therapeutics (San Francisco, CA) through a Materials Transfer Agreement (MTA2018-00000545, 2018) and was diluted in the recommended product formulation buffer for *in vivo* studies.

CRISPR/Cas9-mediated gene knockout

MC38, B16 and YUMMER2.1 murine cell lines were subjected to CRISPR/Cas9-mediated knockout of *B2M* and *JAK1* as previously described (16). The following single guide RNAs targeting *B2M* and *JAK1* were used: forward: 5′-TCACGCCACCCACCGGAGAA-3′ reverse: 5′-TTCTCCGGTGGGTGGCGTGAC-3′ for *B2M*, and forward: 5′-CAGCGGAGAGTATACAGCCG-3′ reverse: 5′-CGGCTGTATACTCTCCGCTG-3′ for

JAK1. These were cloned into the pSpCas9(BB)-2A-GFP vector (Addgene, Watertown, MA, Cat #48138) (18) and then transformed into Stbl3 competent cells (Macro Lab Facility, University of California, Berkeley CA, Cat #Stbl3) and cultured overnight in Lysogeny Broth (LB) (MP Biomedicals, Salem, OR, Cat #113002016) plates containing ampicillin. Selected colonies were grown overnight in LB medium and DNA was isolated with the QIAprep midiprep kit (Qiagen, Valencia, CA, Cat #27104). To verify the sequence of the plasmids, a U6 promoter primer forward 5′-GCCTATTTCCCATGATTCCTTC-3′ was utilized. Next, cells were transfected using Lipofectamine 3000 following the manufacturer's protocol (Thermo Fisher Scientific, Waltham, MA, Cat #L3000001), and GFP-positive cells were collected and single-cell sorted 48 to 72 hours post-transfection at the UCLA Jonsson Comprehensive Cancer Center (JCCC) Flow Cytometry Core. For each clone, genomic DNA was isolated using the NucleoSpin Tissue XS kit (Macherey-Nagel Düren, Nordrhein-Westfalen, Germany, Cat #740901.50), and a 700-base pair (bp) region including the sgRNA was amplified via PCR using HotStarTaq Master Mix (Qiagen, Cat #203446). Finally, disruption was verified by Sanger sequencing utilizing the Tracking of Indels by Decomposition (TIDE) (19) web tool and further confirmed via Western blot.

Western blotting

Selected cell lines were maintained in 10-cm culture dishes and analyzed when 70%–80% confluent. Western blot analysis was performed as described previously (16). Primary antibodies were specific for B2M (clone EP2978Y, ref 75853, Abcam, Cambridge, UK) and GAPDH (clone D16H11, Cell Signaling Technology, Danvers, MA, Cat #5174). Immunoreactivity was analyzed with the ECL-Plus Kit (Amersham Biosciences Co., Buckinghamshire, UK) using the ChemiDoc MP System (Bio-Rad Laboratories, Hercules, CA).

Surface flow cytometry analysis of PD-L1 and MHC class I

On day 1, murine cancer cell lines (B16, MC38 and YUMMER2.1) were plated at 2×10^5 per 6-well plate and, when cell confluence reached 70–80%, cells were collected for surface staining. The day after, culture media was replaced with fresh media with or without IFNγ 100 ng/ml (PeproTech, Cat #315-015) for 18 hours. On day 3 after incubation, cells were trypsinized and then incubated at 37°C for 2 hours with the same concentrations of IFNγ. Next, cells were centrifuged to remove the media and resuspended in 100% FBS. Cells were first stained with Zombie Green viability dye (BioLegend, San Diego, CA Cat #423111) for 15 minutes, then washed and stained with PE-conjugated anti-mouse PD-L1 (clone MIH5, BD Biosciences, Cat #558091), APC-conjugated anti-mouse MHC I (clone 28-14-8, eBioscience, Cat #17-5999-82) and AF700-conjugated anti-mouse MHC II (clone M5, eBioscience, Cat #56-5321-82), and left on ice for 20 minutes. Cells were then washed once with 3 ml PBS and resuspended in 300 μL of PBS. Following staining, samples were analyzed using the Attune Flow Cytometer (Thermo Fisher Scientific) platform at the UCLA JCCC Flow Cytometry Core. Data were analyzed using FlowJo software (version 10.0.8r1, Tree Star Inc., San Carlos, CA). Experiments were performed at least in duplicate per cell line.

Antitumor studies in mouse models

To seed subcutaneous (s.c.) tumors in mice, 0.3×10^6 MC38, 0.3×10^6 B16, or 1×10^6 YUMMER2.1 wild-type or established *B2M*-KO cells were injected into the flanks of female C57BL/6N mice (6–10 weeks of age). Once tumors became palpable, four to six doses of 300 μg of anti–PD-1 or isotype control antibody were injected intraperitoneally (i.p.) every 3 days. Bempegaldesleukin was injected at 0.8 mg/kg every 9 days for one to two doses intravenously (tail vein). For depletion studies, 300 μg of anti-CD8, 300 μg of anti-CD4, 300 μg of anti-NK1.1, 200 μg of anti-CD40L, 200 μg of anti-IFNγ or various combinations were administered every 3 days starting the day before anti–PD-1 or bempegaldesleukin treatment and up until the end of the experiment. To validate depletion efficacy, splenocytes from control and depleted corresponding mice were harvested for comparison by flow cytometric analysis. Tumor growth was followed using caliper measurements two or three times per week and tumor volume was calculated using the following formula: tumor volume= ((width)2 x length)/2. Mean and standard error of the tumor volumes per group was calculated.

Characterization of the tumor immune infiltrate by flow cytometry

To characterize and quantify the dendritic-cell (DC), T cell and myeloid cell populations, mouse tumor samples were collected at day 9 and day 16 after mice were inoculated with MC38 wild-type (WT) or *B2M*-KO cells and treated with anti–PD-1 or isotype. Tumor samples were processed using the mouse tumor dissociation kit (Miltenyi, Bergisch Gladbach, Germany, Cat #130-096-730) per the manufacturer's protocol. Samples were stained using the three antibody panels listed in Supplementary Table S1. Following staining, samples were analyzed using the LSRII (Becton, Dickinson and Company, Franklin Lakes, NJ) at the UCLA JCCC Flow Cytometry Core and analyzed using FlowJo software (version 10.0.8r1, Tree Star Inc., San Carlos, CA).

Mass cytometry by time of flight (CyTOF) analysis

A total of 0.3×10^6 MC38 wild-type or established *JAK1* and *B2M* KO tumor cells were implanted into the flanks of C57BL/6N mice. On day 13 post-implantation, tumors were harvested from mice that had received predefined treatments. Tumors were digested using the mouse tumor dissociation kit (Miltenyi, Cat #130-096-730). Spleens were dissociated and filtered using a 70-μm filter, followed by digestion with the ACK lysis buffer (Lonza, Cat #BP10-548E). Sample staining and data acquisition were performed as previously described with the additional modifications that 3% paraformaldehyde was utilized and samples were not barcoded (16). The immune marker panel has been previously described (16). Samples were analyzed using the Fluidigm Helios (San Francisco, CA) mass cytometry system at the UCLA JCCC Flow Cytometry Core. Samples were manually gated for cells, singlets and double expression of the viable CD45 single-cell-positive population using FlowJo software (version 10.4.2), and data files were analyzed using the standard settings in OMIQ data analysis software (www.omiq.ai).

Clinical dataset

For human tumor biopsy analyses, a clinical dataset of patients with advanced melanoma (n=514) that has been previously harmonized for somatic variant detection and gene expression profiling was utilized (21). This dataset contains clinical response, whole-exome sequencing (WES), and bulk RNA-sequencing (RNAseq) data across seven clinical trials of patients with advanced melanoma who received ICB therapy (anti–PD-1, anti–CTLA-4, or combination therapy). Copy number alterations (CNAs), loss of heterozygosity (LOH), and tumor purity estimates were determined using Sequenza (22). For gene expression analysis, the normalized log-CPM file that was batch-effect corrected with ComBat-seq was utilized (23).

Among the seven clinical trials, the Liu cohort (24), CheckMate 038 (9), CheckMate 064 (25), and CheckMate 067 (26) cohorts were further analyzed since these are the only trials that have both WES and RNAseq data (Supplementary Figure S1). For these analyses, pretreatment melanoma tumors of cutaneous, mucosal, acral, unknown, and uveal origins were utilized. Samples with best overall response (BOR) categories of complete response (CR), partial response (PR), and progressive disease (PD) to ICB therapy were used for clinical response group comparisons, with CR/PR representing clinical responders and PD representing clinical non-responders (RECIST v1.1 criteria) (27). Stable disease (SD) tumors were excluded from clinical response group comparisons but included in somatic variant analysis.

B2M genetic alteration analysis

Using the WES data (see Clinical dataset) of samples with greater than 10% tumor purity, baseline tumors were analyzed for *B2M* genetic alterations (n=295) (Supplementary Table S2). Tumors were considered *B2M* altered if they had non-silent mutations, CNAs, or LOH at the *B2M* locus. Non-silent mutations correspond to single nucleotide variants (SNVs) and insertions and deletions (indels) with a high or moderate Ensembl VEP impact designation (https://uswest.ensembl.org/index.html). CNAs refer to somatic alterations that result in gained or lost copies of a genetic region. LOH describes events where one copy of an allele is lost, irrespective of copy number status. For *B2M* group comparisons, tumors with *B2M* gains were excluded since they do not correspond to downregulating *B2M* genetic alterations. Additionally, SD tumors were excluded from the dataset for clearer responder versus non-responder comparisons (Supplementary Figure S1).

Tumor microenvironment analysis

Immune cell deconvolution of RNASeq data (see Clinical dataset) was performed with CIBERSORTx (https://cibersortx.stanford.edu) using the LM22 signature matrix of 22 functionally defined mature human immune cell subsets (28–30), which distinguishes different cell types and cell states (naïve, memory, resting, and activated) based on 547 significantly differentially expressed genes (Supplementary Table S3). Each cohort was run separately using the uncorrected RNAseq FPKM values to infer cell fractions and total cell numbers (absolute mode) per tumor sample (Supplementary Table S4). Each job was run following the recommended parameters using 1,000 permutations. The p-values calculated by CIBERSORTx ranged from 0 to 0.857 in regular mode (median 0.065) and 0 to 0.836

(median 0.075) in absolute mode (Supplementary Figure S2), and these values were loosely correlated with estimated tumor purity by Sequenza (WES) (Supplementary Figure S3). We performed comparisons of immune cell types across clinical groups two ways: all samples or excluding samples with p>0.5. The significance in comparison across immune cell types was not different across these analyses, so the findings from the first comparison, including all samples, was reported. Differences in immune cell populations between groups were visualized and evaluated in R/RStudio (http://www.R-project.org/) by comparing the medians using a Wilcoxon test and were considered significantly different if the p-value was less than 0.05.

Bioinformatics statistical analysis

Statistical analyses were performed using R/RStudio (v2022.07.1+554, http://www.R-project.org/). All plots analyzing *B2M* groups were generated using the R package ggplot2 (https://ggplot2.tidyverse.org/). For median group comparisons, p-values less than 0.05 were considered statistically significant.

Data availability

The genomics data used in this study are from a previous publication (21), with the raw sequencing data available through the Sequence Read Archive accession identifier PRJNA923698. Processed data from the harmonized biopsy sequencing dataset, including annotated variants and gene expression values, are available at https://github.com/ParkerICI/MORRISON-1-public. All other data generated in this study are available within the article and its Supplementary Data Files or upon request from the corresponding author.

Results

Different constitutive and induced MHC class I expression on MC38, B16 and YUMMER 2.1

Cancer cell lines have different levels of constitutive surface MHC class I expression and frequently do not express MHC class II, but both can be increased by exposure to IFNγ. Thus, using flow cytometry we characterized the baseline and inducible surface expression of MHC class I and II on three murine cell lines, MC38, B16, and YUMMER 2.1. We also analyzed expression of PD-L1 as it is readily induced by IFNγ (31). To determine the role of B2M in modulating the expression of these surface markers, we generated corresponding *B2M*-KO sublines using CRISPR/Cas9 gene editing (16). Constitutive MHC class I surface expression was highest in MC38, intermediate in YUMMER2.1 and lowest in B16 (Figure 1). The same trend was observed when staining for the constitutive surface expression of MHC class II. Exposure to IFNγ resulted in increased MHC class I and II expression in the three models. In all three models, *B2M* KO led to the loss of surface expression of both MHC class I and II, but maintained the upregulation of surface expression of PD-L1 in response to IFNγ (Figure 1). We reasoned that these different levels of MHC class I expression may result in different sensitivities to effector immune cells *in vivo*, as MHC class I is required for tumor recognition by $CD8^+$ T cells, and loss of MHC class I sensitizes target cells to NK-cell cytotoxicity.

CD4+ T cells are instrumental in controlling MC38 *B2M*-deficient tumor growth

To analyze the role of effector immune cell subsets in antitumor responses to MC38 murine colon adenocarcinoma tumors, we inoculated C57BL/6N mice with MC38 WT or MC38 *B2M*-KO tumors, followed by antibody-mediated $CD4^+$ T-cell and/or $CD8^+$ T-cell depletion in both groups, and antibody-mediated $NK1.1^+$-cell depletion in *B2M*-KO tumors. In the MC38 WT control group, depletion of $CD4^+$ T cells, $CD8^+$ T cells, or both, abrogated the anti–PD-1 therapy antitumor response, while for WT untreated tumors, there were no significant effects with depletion of either immune cell subset (Figure 2A). On the other hand, MC38 *B2M*-KO tumors did not respond to anti–PD-1 therapy. Untreated MC38 *B2M*-KO tumors grew with similar kinetics as the WT control group, but $CD4^+$ T-cell depletion led to significant tumor overgrowth of MC38 *B2M*-KO tumors for both untreated and treated with anti–PD-1 therapy groups (Figure 2B). NK-cell depletion in MC38 *B2M*-KO tumors had a lower impact, both in tumor growth and in response to anti–PD-1 therapy. Therefore, $CD4^+$ T cells are critical for controlling the growth of MC38 *B2M*-KO tumors regardless of antitumor treatment.

cDC1 but not cDC2 are reduced in MC38 *B2M*-deficient tumors

To analyze the immune cells infiltrating MC38 WT and MC38 *B2M*-KO tumors, mice were inoculated with MC38 WT or MC38 *B2M*-KO lines and treated with isotype control or anti–PD-1 antibody (n=3 mice per group). We harvested spleens and tumors nine and 16 days after tumor inoculation and studied the cell populations by multiplex flow cytometry (Supplementary Figure S4). Regardless of the anti–PD-1 treatment status, no differences were observed in the infiltration by $CD4^+$ T cells, T regulatory cells (Tregs), $CD8^+$ T cells or NK cells (Supplementary Figure S5A). The percentage of $CD62L^+CD44^+$ central memory $CD4^+$ T cells was significantly higher in MC38 *B2M*-KO tumors compared to MC38 WT tumors at day 9 post tumor-cell inoculation. The percentages of $CD8^+PD1^+$, $CD8^+Ki67^+$ and $CD62L^-CD44^+$ effector $CD8^+$ T cells were significantly decreased in MC38 *B2M*-KO tumors compared to MC38 WT tumors at day 16 post tumor-cell inoculation (Supplementary Figure S5A), indicating that T-cell proliferation is occurring in favor of $CD4^+$ T cells (without Tregs) over $CD8^+$ T cells in MC38 *B2M*-KO tumors.

No significant differences in the percentages of tumor-associated macrophages (TAMs), M1 macrophages, M2 macrophages, $CD4^+$ or $CD8^+$ T cells per gram were observed at day 9 (Supplementary Figure S5B and S5C). However, M1 macrophage infiltration and the M1/M2 ratio were significantly decreased at day 16 in the MC38 *B2M*-KO tumors (anti–PD-1 resistant tumors) compared to MC38 WT tumors (Supplementary Figure S5B). Additionally, the number of NK cells per gram at day 9 in MC38 *B2M*-KO tumors was significantly lower relative to WT tumors (Supplementary Figure S5C). In the MC38 *B2M*-KO tumors, we observed a sharp decrease in the percentage of type 1 conventional DCs (cDC1) (migratory $CD11c^{int}$MHC-$II^{hi}CD103^+$DCs and resident $CD11c^{hi}$MHC-$II^{int}CD8a^+$DCs), a subset of DCs that are specialized in priming $CD8^+$ T-cell responses through cross-presentation (32). In contrast, MC38 *B2M*-KO tumors had an increased percentage of type 2 conventional DCs (cDC2), resident $CD11c^{hi}$MHC-$II^{int}CD11b^+$ DCs (Figure 3 and Supplementary Figure S5B). These data suggest that loss of *B2M* in MC38 tumors abrogates the activation and migration of cDC1 regardless of

anti–PD-1 treatment and promotes attraction of cDC2, which are more potent activators of $CD4^+$ T cells, into the tumor microenvironment (32).

$CD4^+$ T cells and NK cells increase while cDC1 $CD103^+$ cells decrease in MC38 *B2M*-KO tumors treated with an IL2 pathway agonist

We demonstrated previously that treatment with the CD122-preferential IL2 agonist bempegaldesleukin alone or in combination with anti–PD-1 overcame therapeutic resistance to anti–PD-1 therapy in MC38 *B2M*-KO tumors (16). In the prior study, depletion analyses suggested that NK and $CD4^+$ T cells, which are not restricted by MHC class I, played a key role in this antitumor immunity. We also demonstrated that despite tumor-intrinsic IFNγ defects, MC38 *JAK1*-KO tumors with sufficient basal expression of MHC class I could overcome anti–PD-1 therapy resistance with Toll-like receptor 9 (TLR9) agonist co-administration, an effect mediated mainly by $CD8^+$ T cells. Both loss and downregulation of MHC class I antigen presentation are considered major immune escape mechanisms (6–8), but they have varying effects on effector immune cells. Thus, we here used CyTOF analysis of the tumor microenvironment to characterize the effects of bempegaldesleukin and anti–PD-1 plus bempegaldesleukin on the immunological response changes in MC38 WT, MC38 *B2M*-KO, and MC38 *JAK1*-KO tumors, as these readily respond to bempegaldesleukin combined with anti–PD-1 (Supplementary Figure S6). At 13 days post-tumor inoculation, the combination of bempegaldesleukin with anti–PD-1 led to increased $CD4^+$ T cells and NK cells and reduced $CD8^+$ T cells in MC38 *B2M*-KO tumors (Figure 4). In contrast, $CD8^+$ T, $CD4^+$ T and NK cells all increased in bempegaldesleukin and anti–PD-1-treated MC38 *JAK1*-KO tumors (Figure 4). This is consistent with our previous findings in which $CD8^+$ T cells were the main immune effectors in MC38 *JAK1*-KO tumors with sufficient basal MHC class I expression (16). $CD103^+$ murine DCs decreased in MC38 *B2M*-KO tumors regardless of treatment (Figure 3A, Figure 4C, and Supplementary Figure S7A). On the other hand, bempegaldesleukin significantly expanded $CD103^+$ murine DCs, which are required for cross-presentation, in both MC38 WT and *JAK1*-KO tumors. Altogether, our results support that the infiltration of cDC1 $CD103^+$ murine DCs decreases in MC38 *B2M*-KO tumors regardless of treatment, and that anti–PD-1 therapy resistance can be overcome with an IL2 pathway agonist by activating $CD4^+$ T-cell and NK-cell responses.

Depletion of $CD4^+$ T cells promotes pro-tumorigenic macrophage differentiation

Because our data suggested that $CD4^+$ T cells played a key role in MC38 *B2M*-KO tumors, we further explored the role that tumor-infiltrating $CD4^+$ T cells may play in determining macrophage differentiation. While bempegaldesleukin treatment led to a minimal expansion of tumor-associated macrophages (TAM), isotype control and bempegaldesleukin with $CD4^+$ T-cell depletion (where tumors grew faster) led to a dramatic increase in macrophages (Supplementary Figure S7B). Additionally, immunosuppressive M2 macrophages were significantly increased in bempegaldesleukin with $CD4^+$ T-cell depletion, with a decrease in the M1/M2 index at day 13 after tumor inoculation. These data suggest that $CD4^+$ T cells limit macrophage differentiation and/or proliferation toward an immunosuppressive M2 state.

NK cells and IFNγ control tumor growth in B16 *B2M*-KO tumors

B16 murine melanoma has low basal expression of MHC class I, which can be increased with IFNγ exposure (33), and is mainly dependent on $CD8^+$ T cells for the antitumor response in the setting of anti–PD-L1 therapy (34). . Our prior work showed that in B16 *B2M*-KO tumors, bempegaldesleukin or bempegaldesleukin in combination with anti–PD-1 overcame therapeutic resistance to anti–PD-1 (16). Herein, we investigated the cell types responsible for the antitumor activity of bempegaldesleukin in B16 *B2M*-KO tumors. Depletion of NK cells abolished the therapeutic effect of the IL2 agonist (Figure 5). In contrast, depletion of $CD4^+$ or $CD8^+$ T cells had no effect. We further studied the molecules involved in the immune cell interactions by administering blocking antibodies against IFNγ or CD40L. We observed that the antitumor activity of bempegaldesleukin was lost when blocking IFNγ, but not when blocking CD40L (Figure 5), which is canonically expressed on $CD4^+$ T cells and plays an important role in the T cell–mediated activation of DCs (35,36). These data suggest that NK cells and IFNγ are essential for overcoming anti–PD-1 therapy resistance in B16 *B2M*-KO tumors. In addition, these results show that $CD4^+$ T cells and T-cell help through CD40L were not crucial for developing an effective antitumor immune response in this model.

YUMMER2.1 *B2M*-KO tumors respond to anti–PD-1 therapy

The YUMM2.1 murine melanoma cell line provides a $BRAF^{V600E}/PTEN$-null-driven model that has been previously shown to be responsive to anti–PD-1 therapy (37), with $CD4^+$ T-cell depletion completely abrogating the antitumor effect and $CD8^+$ T-cell depletion only having a partial effect (17). To generate a model that not only included melanoma driver oncogenes but also had increased ultraviolet (UV) light–induced mutational burden, as it is frequently found in human cutaneous melanomas (38), we obtained a polyclonal YUMM2.1 by UV exposure and expanded single cell clones to generate 24 UV-homogeneous sublines. This resulted in sublines with truncal UV-induced mutations able to respond to anti–PD-1 therapies (39). We evaluated the *in vitro* and *in vivo* growth curves of the 24 UV-homogeneous sublines in order to identify the subline that behaved most similarly to the parental UV-heterogeneous cell line to select for subsequent *in vivo* studies (Supplementary Figure S8). The resulting YUMM2.1 UV-clone 2, named YUMMER2.1, is a model that more closely resembles human melanomas with $BRAF^{V600E}$ and $PTEN^{-/-}$ oncogenic driver alterations, a high mutational load induced by UV carcinogenesis, and anti–PD-1 therapy responsiveness (Figure 6A–B). Next, we generated a *B2M*-KO subline of YUMMER2.1 using CRISPR/Cas9 gene editing and validated the phenotype by protein analysis (Supplementary Figure S8). To model the *in vivo* response to PD-1 blockade in YUMMER2.1 *B2M*-deficient tumors, we injected YUMMER2.1 *B2M*-KO tumors subcutaneously into the lower flank of C57BL/6N mice. When tumors became palpable, mice received the first out of six injections of anti–PD-1 therapy or isotype control. Even with *B2M* loss, YUMMER2.1 *B2M*-KO tumors responded to anti–PD-1 therapy, showing that this model is largely sensitive to PD-1 blockade treatment (Figure 6C).

Depletion of CD4+ T cells, NK cells, and CD40L abrogates anti–PD-1 therapy response in YUMMER2.1 *B2M*-KO tumors

To investigate the cell types responsible for the anti–PD-1 response in YUMMER2.1 *B2M*-KO tumors, we depleted $CD4^+$ T cells, $CD8^+$ T cells, NK cells, CD40L, and IFNγ. In agreement with previous data with YUMM2.1 (17), $CD8^+$ T-cell depletion only partially abrogated the response, whereas $CD4^+$ T-cell depletion and CD40L blockade completely abrogated the anti–PD-1 therapy response in YUMMER2.1 tumors (Figure 6D–E). Depletion of $CD4^+$ T cells, NK cells and CD40L, but not $CD8^+$ T cells or IFNγ, significantly curbed tumor growth inhibition by anti–PD-1 therapy (Figure 6F–G). These results suggest that in YUMMER2.1 *B2M*-KO tumors, $CD4^+$ T cells and NK cells are the main cells responsible and necessary for anti–PD-1 antitumor activity. Additionally, we further identified the involvement of CD40L in the antitumor response in this *B2M*-deficient murine model.

In human melanoma biopsies, *B2M* LOH is the most prevalent downregulating genetic alteration

We next wanted to study the immune cells infiltrating human melanoma biopsies with and without *B2M* downregulation or complete loss. To determine the *B2M* genetic status in biopsies of patients with advanced melanoma who received ICB therapy, we analyzed data from a harmonized clinical cohort (21). Baseline WES samples (n=295) (Supplementary Table S2 and Supplementary Figure S1) were analyzed for the presence of *B2M* somatic alterations, specifically non-silent mutations, copy number alterations, or loss of heterozygosity (LOH). We found that none of the patients in this cohort had tumors with non-silent mutations in *B2M* (Supplementary Figure S9). However, 49.5% of the cohort (n=146) had tumors with copy number alterations in *B2M*. Of the 295 patients analyzed, 0.7% of patients had biopsies with *B2M* homozygous loss (n=2), 19% had *B2M* LOH with total copy numbers ranging from 1–5 (n=56), and 30% had *B2M* copy number gains with total copy numbers ranging from three to seven (n=88) (Supplementary Figure S9).

B2M LOH in melanoma correlates with progressive disease status and decreased *B2M* expression

In order to elucidate the effects of downregulating *B2M* genetic alterations in the context of clinical response, we compared the clinical outcomes of patients whose tumors had *B2M* homozygous loss or LOH and unaltered status using the response RECIST criteria v1.1 (27), separating patients with complete and partial response (CR/PR) from patients with disease progression (PD) following ICB therapy. This criterion, however, eliminated the two cases with stable disease and *B2M* homozygous loss (Supplementary Figure S9), leaving only *B2M* LOH (n=45) and unaltered tumors (n=119) for analysis (Supplementary Figure S1). We found that the presence of *B2M* LOH events in progressive disease tumors (n=32/95) was significantly higher compared to responsive tumors (n=13/69), occurring approximately twice as often in biopsies of patients with no response to therapy (34% versus 19%; X^2_{Pearson} test, p=0.04) (Figure 7A). Next, to determine whether *B2M* LOH was associated with reduced *B2M* expression, bulk tumor RNAseq data (n=100) was analyzed for *B2M* expression differences (Supplementary Figure S1). We found that *B2M* expression

was lower in *B2M* LOH tumors compared to unaltered tumors (Wilcoxon test, p=0.05) (Figure 7B). These results agree with prior studies that describe *B2M* LOH events as potential precursors to *B2M* loss and thus, reduced *B2M* expression (7).

Melanomas with *B2M* LOH have more activated NK cells

To determine the immune cell subtypes present in *B2M* LOH (n=25) versus unaltered tumors (n=75), we performed immune cell deconvolution analysis on samples with paired WES and RNAseq data using CIBERSORTx (https://cibersortx.stanford.edu). We found that *B2M* LOH tumors had significantly higher fractions (Wilcoxon test, p=0.032) and quantified amounts (Wilcoxon test, p=0.021) of activated NK cells (Figure 7C and Supplementary Figure S10A). It is also worth noting that compared to unaltered tumors, *B2M* LOH tumors had trends supporting greater fractions and numbers of M1 macrophages, γδ T cells, memory resting $CD4^+$ T cells, plasma cells, memory B cells, $CD8^+$ T cells, activated mast cells, and follicular helper T cells (Figure 7C and Supplementary Figure S10A).

Furthermore, when examining the immune cell composition of *B2M* LOH tumors across ICB response groups, the fractions of monocytes were significantly higher in *B2M* LOH responsive tumors (n=6, Wilcoxon test, p=0.026), while the fractions of memory activated $CD4^+$ T cells were significantly higher in *B2M* LOH progressive tumors (n=19, Wilcoxon test, p=0.014) (Figure 7D). These patterns were also observed with the absolute scores, where only monocytes and memory activated $CD4^+$ T cells were significantly different between both groups (Supplementary Figure S10B). Notably, *B2M* LOH progressive tumors also had greater fraction and absolute score values for activated NK cells, γδ T cells, and $CD8^+$ T cells; and a greater absolute score value for M1 macrophages (Figure 7D and Supplementary Figure S10B).

Next, to assess which subsets may be playing a more prominent role in mediating response to ICB therapy, we focused exclusively on responsive (CR/PR) melanoma tumors, comparing the estimated immune cell populations between *B2M* LOH tumors (n=6) and *B2M* unaltered tumors (n=35). It was observed that compared to unaltered samples, only monocytes were significantly higher in *B2M* LOH responsive tumors for both fractions (Wilcoxon test, p=0.018) and absolute values (Wilcoxon test, p=0.03) (Supplementary Figure S11). However, it is also important to note that *B2M* LOH responsive tumors had higher fractions and total numbers of activated NK cells and memory resting $CD4^+$ T cells relative to *B2M* unaltered tumors (Supplementary Figure S11). Our results indicate that in human melanoma biopsies with *B2M* dysregulation, activated NK cells are the most significantly elevated immune cell type infiltrating the tumors, with potential roles for other immune cells, such as $CD4^+$ T cells, monocytes/M1 macrophages, and γδ T cells.

Discussion

It has been well-documented that cancers with *B2M* homozygous loss could still respond to PD-1 blockade–based therapies (9–15), which challenges the conventional thinking on the mode of action of anti–PD-1 by reinvigorating cytotoxic $CD8^+$ T cells that recognize tumor antigens presented by MHC class I (2). The effector arm of a cellular antitumor immune response has two main cytotoxic cells, $CD8^+$ T cells recognizing MHC class I antigen

complexes and NK cells recognizing the absence of or a mismatched MHC class I. The need to avoid NK-cell killing seems to be a major driver for cancers to not lose MHC class I expression completely (40), even if this would allow the cancer to acquire resistance to ICB therapies (6–8). In addition, $CD4^+$ T cells can have effector functions that induce cytotoxic cancer cell death, either directly or indirectly through the secretion of cytokines that promote bystander cytotoxicity. Furthermore, the helper function of $CD4^+$ T cells, which involves cytokines such as IFNγ and CD40L engagement through DCs, results in increased cytotoxic activity of $CD8^+$ T cells and NK cells (41).

We reasoned that identifying the immune cell mediators capable of exerting the antitumorigenic effects of anti–PD-1 therapy response in the absence of *B2M* is of critical importance in order to not only address antigen presentation-mediated therapeutic resistance, but also to better understand the mechanism of action of PD-1 blockade therapies. In this study, we used a combination of three different murine models with varying immune cell dependencies and human melanoma biopsy samples to interrogate the dominant immune cell subtypes and molecular markers associated with the immune response of *B2M*-deficient tumors. The YUMMER2.1 model is highly immunogenic and is able to respond to anti–PD-1 therapy, even in the absence of MHC class I presentation due to *B2M* loss, through $CD4^+$ T cell and T-cell helper functions. The MC38 model has intermediate immunogenicity and does not respond to anti–PD-1 single agent therapy when there is no MHC class I presentation. However, it can respond to therapy adding an IL2 pathway agonist, and in this case, the antitumor response is mediated by $CD4^+$ T cells and NK cells, with a critical requirement for T-cell help and intratumoral DCs. The low immunogenicity B16 model is resistant to anti–PD-1 with or without *B2M* loss, but can respond with an IL2 pathway agonist and the response is completely dependent on NK cells with no added role for $CD4^+$ T cells or T-cell helper functions. Our work in murine models has shown that $CD4^+$ T cells are critical for the antitumor immunity in *B2M*-KO models. This is opposite of what has been reported in prior studies where it was observed that $CD4^+$ T-cell depletion led to increased tumor reactivity and increased intratumoral infiltration of $CD8^+$ T cells (42,43). However, in our models Tregs are not expected to play a significant role in tumor reactivity and response, as demonstrated by the MC38 line where WT and *B2M*-KO tumors had similar quantities of Tregs; thus, depleting $CD4^+$ T cells in this scenario would not decrease the amount of immunosuppressive $CD4^+$ T cells in the tumor microenvironment. Furthermore, since these are *B2M*-KO lines with a compromised MHC class I–$CD8^+$ T cell immunity axis, an increase in tumor-specific $CD8^+$ T cells due to $CD4^+$ T-cell depletion would not lead to a therapeutic benefit. Our findings in these mouse models highlight the complexity of investigating immune responses in the context of *B2M* loss, stressing that tumor-intrinsic immune cell dependencies as well tumor microenvironmental factors can impact which effector cells control *B2M*-null tumor growth. Nonetheless, our work suggests that NK and $CD4^+$ T cells are the dominant cell types curbing MHC class I–defective tumor expansion.

In our analysis of pretreatment human melanoma biopsies, we identified *B2M* LOH due to copy number alterations as the most prevalent downregulating genetic alteration and found no non-silent mutations in *B2M*, which is in accordance with prior series (7,24). We also observed that *B2M* LOH occurred approximately twice as often in biopsies from

patients who did not respond to ICB therapy compared to those who had a clinical response. This falls in line with what was found in two independent melanoma clinical cohorts, where the frequency of *B2M* LOH events at baseline was roughly three times higher in biopsies of patients with progressive disease (7). Our immune cell deconvolution analysis of *B2M* LOH melanoma biopsies showed that, among the immune cell types analyzed, only activated NK cells were significantly higher in *B2M* LOH tumors when compared to *B2M* unaltered tumors. Additionally, we also observed higher amounts of activated NK cells in *B2M* LOH responsive tumors compared to *B2M* unaltered responsive tumors. This is consistent with the notion that MHC class I loss leaves tumor cells susceptible to NK cell–mediated killing (40,44). Furthermore, this is consistent with similar work analyzing the transcriptional profiles of two datasets of patients with non-small cell lung cancer (NSCLC) comparing tumors with low *B2M* expression against tumors with high *B2M* expression, where the fraction of activated NK cells was higher in *B2M*-low tumors (45). These results lend support toward NK cells potentially being the main mediators of MHC class I–negative tumor removal. We hypothesize that low or lost MHC class I expression in tumors leads to NK-cell activation. However, despite the greater numbers and proportions of activated NK cells found in *B2M* LOH melanomas, these biopsies were still associated with progressive disease, and it was the *B2M* LOH progressive tumors that had the greatest amount of activated NK cells and other cytotoxic immune cell types. This suggests that there may be inhibitory molecules present in the tumor microenvironment that are impeding NK-cell cytotoxic activity, stressing the need for more in-depth studies into the tumor microenvironment of *B2M*-dysregulated tumors. Additionally, in our samples, we found that M1 macrophages, memory resting $CD4^+$ T cells, and γδ T cells were higher in *B2M* LOH tumors, with responsive tumors having greater amounts of monocytes and memory resting $CD4^+$ T cells. Another striking observation since, as demonstrated by our murine models and previous studies, M1 macrophages that are no longer inhibited by the interaction of B2M with LILRB1 (46), and $CD4^+$ T cells that are not dependent on surface MHC class I expression (13), can also play a role in eradicating *B2M*-null tumors. Similarly, it has recently been shown that γδ T cells, which are also not restricted by surface MHC class I expression, had high infiltration rates in *B2M*-inactivated MMR-d cancers and were associated with enhanced reactivity and cytotoxic activity against MHC class I–negative tumors (15).

In conclusion, cancers may induce different immune cell subset responses depending on their inherent immunogenicity and the level of surface MHC class I expression. The main immune cell subset mediating antitumor responses induced by PD-1 blockade in humans are $CD8^+$ T cells (1), with the need for costimulation and help from $CD4^+$ T cells when using PD-1 blockade therapies in implantable murine models where the immune system needs to be primed to induce tumor regression (17,47,48). As cancers attempt to evade the immune system by decreasing their immunogenicity through decreased tumor antigen presentation by MHC class I downregulation or loss, it triggers an alternate immune surveillance process mediated by NK cells, and potentially γδ T cells, with differing roles for $CD4^+$ T cells depending on the model system.

Supplementary Material

Refer to Web version on PubMed Central for supplementary material.

Acknowledgments

This study was funded in part by the Parker Institute for Cancer Immunotherapy (PICI), NIH grants R35 CA197633 and P01 CA168585, the Ressler Family Fund, and the support from Ken and Donna Schultz, Todd and Donna Jones, Karen and James Witemyre, and Thomas Stutz through the Jonsson Cancer Center Foundation, and Jonathan Isaacson through the Melanoma Research Foundation (to A.R.). D.Y.T was supported by a Young Investigator Award from ASCO, a grant from the Spanish Society of Medical Oncology for Translational Research in Reference Centers and the V Foundation-Gil Nickel Family Endowed Fellowship in Melanoma Research. M.G. is a pre-doctoral fellow supported by the UCLA Tumor Cell Biology Training Program USHHS Ruth L. Kirschstein Institutional National Research Service Award T32 CA009056 and the UCLA Medical Scientist Training Program (MSTP) NIH NIGMS Training Grant T32 GM008042. G.A-R. was supported by the Isabel & Harvey Kibel Fellowship award and the Alan Ghitis Fellowship Award for Melanoma Research. K.M.C. is supported by the Cancer Research Institute Irvington Postdoctoral Fellowship Program, the V Foundation Gil Nickel Melanoma Research Fellowship, and the Parker Institute for Cancer Immunotherapy and V Foundation Bridge Fellows Program. Flow and mass cytometry were performed in the UCLA Jonsson Comprehensive Cancer Center (JCCC) and Center for AIDS Research Flow Cytometry Core Facility that is supported by NIH awards P30 CA016042 and 5P30 AI028697, and by the JCCC, the UCLA AIDS Institute, and the David Geffen School of Medicine at UCLA.

References

1. Tumeh PC, Harview CL, Yearley JH, Shintaku IP, Taylor EJ, Robert L, et al. PD-1 blockade induces responses by inhibiting adaptive immune resistance. Nature 2014;515(7528):568–71 doi 10.1038/nature13954. [PubMed: 25428505]
2. Ribas A, Wolchok JD. Cancer immunotherapy using checkpoint blockade. Science 2018;359(6382):1350–5 doi 10.1126/science.aar4060. [PubMed: 29567705]
3. Ploegh HL, Orr HT, Strominger JL. Major histocompatibility antigens: the human (HLA-A, -B, -C) and murine (H-2K, H-2D) class I molecules. Cell 1981;24(2):287–99 doi 10.1016/0092-8674(81)90318-4. [PubMed: 7016338]
4. D'Urso CM, Wang ZG, Cao Y, Tatake R, Zeff RA, Ferrone S. Lack of HLA class I antigen expression by cultured melanoma cells FO-1 due to a defect in B2m gene expression. J Clin Invest 1991;87(1):284–92. [PubMed: 1898655]
5. Restifo NP, Marincola FM, Kawakami Y, Taubenberger J, Yannelli JR, Rosenberg SA. Loss of functional beta 2-microglobulin in metastatic melanomas from five patients receiving immunotherapy. J Natl Cancer Inst 1996;88(2):100–8. [PubMed: 8537970]
6. Zaretsky JM, Garcia-Diaz A, Shin DS, Escuin-Ordinas H, Hugo W, Hu-Lieskovan S, et al. Mutations Associated with Acquired Resistance to PD-1 Blockade in Melanoma. N Engl J Med 2016;375(9):819–29 doi 10.1056/NEJMoa1604958. [PubMed: 27433843]
7. Sade-Feldman M, Jiao YJ, Chen JH, Rooney MS, Barzily-Rokni M, Eliane JP, et al. Resistance to checkpoint blockade therapy through inactivation of antigen presentation. Nat Commun 2017;8(1):1136 doi 10.1038/s41467-017-01062-w. [PubMed: 29070816]
8. Gettinger S, Choi J, Hastings K, Truini A, Datar I, Sowell R, et al. Impaired HLA Class I Antigen Processing and Presentation as a Mechanism of Acquired Resistance to Immune Checkpoint Inhibitors in Lung Cancer. Cancer Discov 2017 doi 10.1158/2159-8290.CD-17-0593.
9. Riaz N, Havel JJ, Makarov V, Desrichard A, Urba WJ, Sims JS, et al. Tumor and Microenvironment Evolution during Immunotherapy with Nivolumab. Cell 2017;171(4):934–49 e16 doi 10.1016/j.cell.2017.09.028. [PubMed: 29033130]
10. Benci JL, Johnson LR, Choa R, Xu Y, Qiu J, Zhou Z, et al. Opposing Functions of Interferon Coordinate Adaptive and Innate Immune Responses to Cancer Immune Checkpoint Blockade. Cell 2019;178(4):933–48 e14 doi 10.1016/j.cell.2019.07.019. [PubMed: 31398344]
11. Grasso CS, Giannakis M, Wells DK, Hamada T, Mu XJ, Quist M, et al. Genetic Mechanisms of Immune Evasion in Colorectal Cancer. Cancer Discov 2018;8(6):730–49 doi 10.1158/2159-8290.CD-17-1327. [PubMed: 29510987]

12. Keenan TE, Burke KP, Van Allen EM. Genomic correlates of response to immune checkpoint blockade. Nat Med 2019;25(3):389–402 doi 10.1038/s41591-019-0382-x. [PubMed: 30842677]
13. Germano G, Lu S, Rospo G, Lamba S, Rousseau B, Fanelli S, et al. CD4 T Cell-Dependent Rejection of Beta-2 Microglobulin Null Mismatch Repair-Deficient Tumors. Cancer Discov 2021;11(7):1844–59 doi 10.1158/2159-8290.CD-20-0987. [PubMed: 33653693]
14. Middha S, Yaeger R, Shia J, Stadler ZK, King S, Guercio S, et al. Majority of B2M-Mutant and -Deficient Colorectal Carcinomas Achieve Clinical Benefit From Immune Checkpoint Inhibitor Therapy and Are Microsatellite Instability-High. JCO Precis Oncol 2019;3 doi 10.1200/PO.18.00321.
15. de Vries NL, van de Haar J, Veninga V, Chalabi M, Ijsselsteijn ME, van der Ploeg M, et al. gammadelta T cells are effectors of immunotherapy in cancers with HLA class I defects. Nature 2023 doi 10.1038/s41586-022-05593-1.
16. Torrejon DY, Abril-Rodriguez G, Champhekar AS, Tsoi J, Campbell KM, Kalbasi A, et al. Overcoming genetically-based resistance mechanisms to PD-1 blockade. Cancer Discov 2020;(epub):May 28: CD-19-1409. doi: 10.158/2159-8290.
17. Homet Moreno B, Zaretsky JM, Garcia-Diaz A, Tsoi J, Parisi G, Robert L, et al. Response to Programmed Cell Death-1 Blockade in a Murine Melanoma Syngeneic Model Requires Costimulation, CD4, and CD8 T Cells. Cancer immunology research 2016;4(10):845–57 doi 10.1158/2326-6066.CIR-16-0060. [PubMed: 27589875]
18. Ran FA, Hsu PD, Wright J, Agarwala V, Scott DA, Zhang F. Genome engineering using the CRISPR-Cas9 system. Nat Protoc 2013;8(11):2281–308 doi 10.1038/nprot.2013.143. [PubMed: 24157548]
19. Brinkman EK, Chen T, Amendola M, van Steensel B. Easy quantitative assessment of genome editing by sequence trace decomposition. Nucleic Acids Res 2014;42(22):e168 doi 10.1093/nar/gku936. [PubMed: 25300484]
20. Charych DH, Hoch U, Langowski JL, Lee SR, Addepalli MK, Kirk PB, et al. NKTR-214, an Engineered Cytokine with Biased IL2 Receptor Binding, Increased Tumor Exposure, and Marked Efficacy in Mouse Tumor Models. Clin Cancer Res 2016;22(3):680–90 doi 10.1158/1078-0432.CCR-15-1631. [PubMed: 26832745]
21. Campbell KM, Amouzgar M, Pfeiffer SM, Howes TR, Medina E, Travers M, et al. Prior anti-CTLA-4 therapy impacts molecular characteristics associated with anti-PD-1 response in advanced melanoma. Cancer Cell 2023;41(4):791–806 e4 doi 10.1016/j.ccell.2023.03.010. [PubMed: 37037616]
22. Favero F, Joshi T, Marquard AM, Birkbak NJ, Krzystanek M, Li Q, et al. Sequenza: allele-specific copy number and mutation profiles from tumor sequencing data. Ann Oncol 2015;26(1):64–70 doi 10.1093/annonc/mdu479. [PubMed: 25319062]
23. Zhang Y, Parmigiani G, Johnson WE. ComBat-seq: batch effect adjustment for RNA-seq count data. NAR Genom Bioinform 2020;2(3):lqaa078 doi 10.1093/nargab/lqaa078. [PubMed: 33015620]
24. Liu D, Schilling B, Liu D, Sucker A, Livingstone E, Jerby-Amon L, et al. Integrative molecular and clinical modeling of clinical outcomes to PD1 blockade in patients with metastatic melanoma. Nat Med 2019;25(12):1916–27 doi 10.1038/s41591-019-0654-5. [PubMed: 31792460]
25. Weber JS, Gibney G, Sullivan RJ, Sosman JA, Slingluff CL, Lawrence DP Jr., et al. Sequential administration of nivolumab and ipilimumab with a planned switch in patients with advanced melanoma (CheckMate 064): an open-label, randomised, phase 2 trial. Lancet Oncol 2016;17(7):943–55 doi 10.1016/S1470-2045(16)30126-7. [PubMed: 27269740]
26. Wolchok JD, Chiarion-Sileni V, Gonzalez R, Rutkowski P, Grob JJ, Cowey CL, et al. Overall Survival with Combined Nivolumab and Ipilimumab in Advanced Melanoma. N Engl J Med 2017;377(14):1345–56 doi 10.1056/NEJMoa1709684. [PubMed: 28889792]
27. Schwartz LH, Litiere S, de Vries E, Ford R, Gwyther S, Mandrekar S, et al. RECIST 1.1-Update and clarification: From the RECIST committee. Eur J Cancer 2016;62:132–7 doi 10.1016/j.ejca.2016.03.081. [PubMed: 27189322]

28. Chen B, Khodadoust MS, Liu CL, Newman AM, Alizadeh AA. Profiling Tumor Infiltrating Immune Cells with CIBERSORT. Methods Mol Biol 2018;1711:243–59 doi 10.1007/978-1-4939-7493-1_12. [PubMed: 29344893]
29. Newman AM, Liu CL, Green MR, Gentles AJ, Feng W, Xu Y, et al. Robust enumeration of cell subsets from tissue expression profiles. Nat Methods 2015;12(5):453–7 doi 10.1038/nmeth.3337. [PubMed: 25822800]
30. Newman AM, Steen CB, Liu CL, Gentles AJ, Chaudhuri AA, Scherer F, et al. Determining cell type abundance and expression from bulk tissues with digital cytometry. Nat Biotechnol 2019;37(7):773–82 doi 10.1038/s41587-019-0114-2. [PubMed: 31061481]
31. Garcia-Diaz A, Shin DS, Moreno BH, Saco J, Escuin-Ordinas H, Rodriguez GA, et al. Interferon Receptor Signaling Pathways Regulating PD-L1 and PD-L2 Expression. Cell reports 2017;19(6):1189–201 doi 10.1016/j.celrep.2017.04.031. [PubMed: 28494868]
32. Sanchez-Paulete AR, Cueto FJ, Martinez-Lopez M, Labiano S, Morales-Kastresana A, Rodriguez-Ruiz ME, et al. Cancer Immunotherapy with Immunomodulatory Anti-CD137 and Anti-PD-1 Monoclonal Antibodies Requires BATF3-Dependent Dendritic Cells. Cancer Discov 2016;6(1):71–9 doi 10.1158/2159-8290.CD-15-0510. [PubMed: 26493961]
33. Seliger B, Wollscheid U, Momburg F, Blankenstein T, Huber C. Characterization of the major histocompatibility complex class I deficiencies in B16 melanoma cells. Cancer Res 2001;61(3):1095–9. [PubMed: 11221838]
34. Ji S, Lee J, Lee ES, Kim DH, Sin JI. B16 melanoma control by anti-PD-L1 requires CD8+ T cells and NK cells: application of anti-PD-L1 Abs and Trp2 peptide vaccines. Hum Vaccin Immunother 2021;17(7):1910–22 doi 10.1080/21645515.2020.1866951. [PubMed: 33522416]
35. Grewal IS, Foellmer HG, Grewal KD, Xu J, Hardardottir F, Baron JL, et al. Requirement for CD40 ligand in costimulation induction, T cell activation, and experimental allergic encephalomyelitis. Science 1996;273(5283):1864–7. [PubMed: 8791592]
36. Schoenberger SP, Toes RE, van der Voort EI, Offringa R, Melief CJ. T-cell help for cytotoxic T lymphocytes is mediated by CD40-CD40L interactions [see comments]. Nature 1998;393(6684):480–3. [PubMed: 9624005]
37. Meeth K, Wang JX, Micevic G, Damsky W, Bosenberg MW. The YUMM lines: a series of congenic mouse melanoma cell lines with defined genetic alterations. Pigment Cell Melanoma Res 2016;29(5):590–7 doi 10.1111/pcmr.12498. [PubMed: 27287723]
38. Wang J, Perry CJ, Meeth K, Thakral D, Damsky W, Micevic G, et al. UV-induced somatic mutations elicit a functional T cell response in the YUMMER1.7 mouse melanoma model. Pigment Cell Melanoma Res 2017;30(4):428–35 doi 10.1111/pcmr.12591. [PubMed: 28379630]
39. Wolf Y, Bartok O, Patkar S, Eli GB, Cohen S, Litchfield K, et al. UVB-Induced Tumor Heterogeneity Diminishes Immune Response in Melanoma. Cell 2019;179(1):219–35 e21 doi 10.1016/j.cell.2019.08.032. [PubMed: 31522890]
40. Karre K NK cells, MHC class I molecules and the missing self. Scand J Immunol 2002;55(3):221–8. [PubMed: 11940227]
41. Janeway CA, Jr., Bottomly K. Signals and signs for lymphocyte responses. Cell 1994;76(2):275–85. [PubMed: 7904901]
42. Selby MJ, Engelhardt JJ, Johnston RJ, Lu LS, Han M, Thudium K, et al. Preclinical Development of Ipilimumab and Nivolumab Combination Immunotherapy: Mouse Tumor Models, In Vitro Functional Studies, and Cynomolgus Macaque Toxicology. PLoS One 2016;11(9):e0161779 doi 10.1371/journal.pone.0161779. [PubMed: 27610613]
43. Ueha S, Yokochi S, Ishiwata Y, Ogiwara H, Chand K, Nakajima T, et al. Robust Antitumor Effects of Combined Anti-CD4-Depleting Antibody and Anti-PD-1/PD-L1 Immune Checkpoint Antibody Treatment in Mice. Cancer Immunol Res 2015;3(6):631–40 doi 10.1158/2326-6066.CIR-14-0190. [PubMed: 25711759]
44. Freeman AJ, Vervoort SJ, Ramsbottom KM, Kelly MJ, Michie J, Pijpers L, et al. Natural Killer Cells Suppress T Cell-Associated Tumor Immune Evasion. Cell reports 2019;28(11):2784–94 e5 doi 10.1016/j.celrep.2019.08.017. [PubMed: 31509742]

45. Zhao Y, Cao Y, Chen Y, Wu L, Hang H, Jiang C, et al. B2M gene expression shapes the immune landscape of lung adenocarcinoma and determines the response to immunotherapy. Immunology 2021;164(3):507–23 doi 10.1111/imm.13384. [PubMed: 34115389]

46. Barkal AA, Weiskopf K, Kao KS, Gordon SR, Rosental B, Yiu YY, et al. Engagement of MHC class I by the inhibitory receptor LILRB1 suppresses macrophages and is a target of cancer immunotherapy. Nat Immunol 2018;19(1):76–84 doi 10.1038/s41590-017-0004-z. [PubMed: 29180808]

47. Kamphorst AO, Wieland A, Nasti T, Yang S, Zhang R, Barber DL, et al. Rescue of exhausted CD8 T cells by PD-1-targeted therapies is CD28-dependent. Science 2017;355(6332):1423–7 doi 10.1126/science.aaf0683. [PubMed: 28280249]

48. Hui E, Cheung J, Zhu J, Su X, Taylor MJ, Wallweber HA, et al. T cell costimulatory receptor CD28 is a primary target for PD-1-mediated inhibition. Science 2017;355(6332):1428–33 doi 10.1126/science.aaf1292. [PubMed: 28280247]

Synopsis:

By studying how antitumor immune responses can be mediated against cancers that are B2M-deficient, and therefore cannot be recognized by cytotoxic CD8+ T cells, the authors provide new understanding of the mechanism of action of ICB therapies.

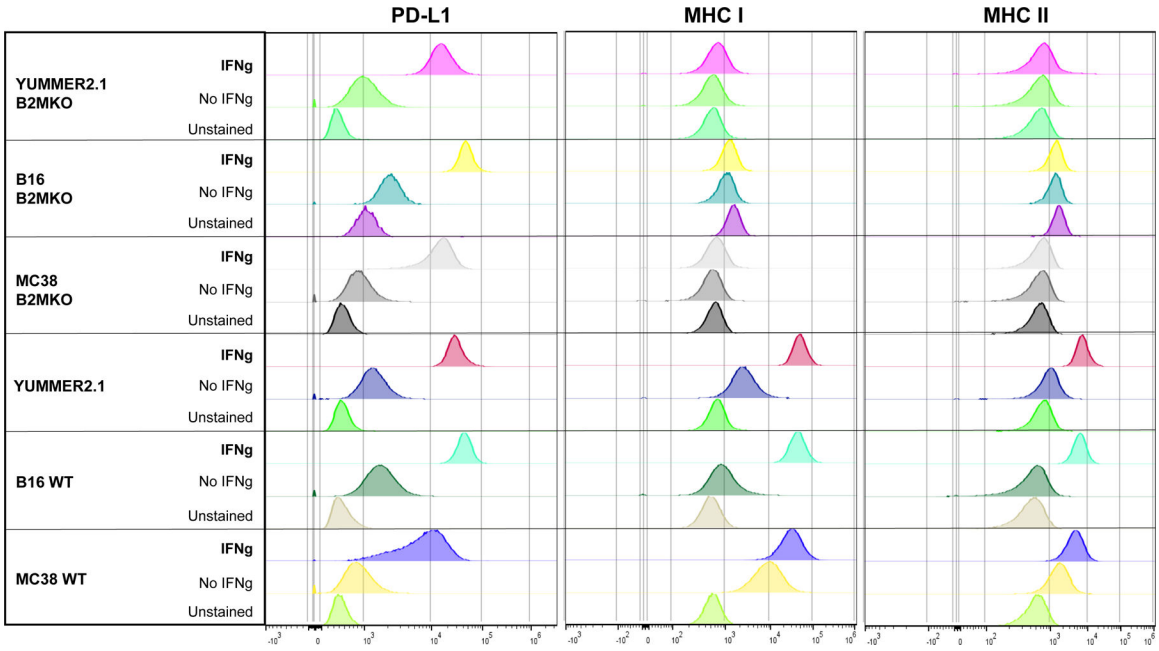

Figure 1. Surface expression of PD-L1, MHC class I and II in murine cell lines.

Wild-type (WT) and *B2M*-knockout (KO) sublines of MC38, B16 and YUMMER2.1 were stained for flow cytometry analysis with and without IFNγ stimulation. Histograms represent changes in mean fluorescence intensity (MFI) by flow cytometry compared with unstained control.

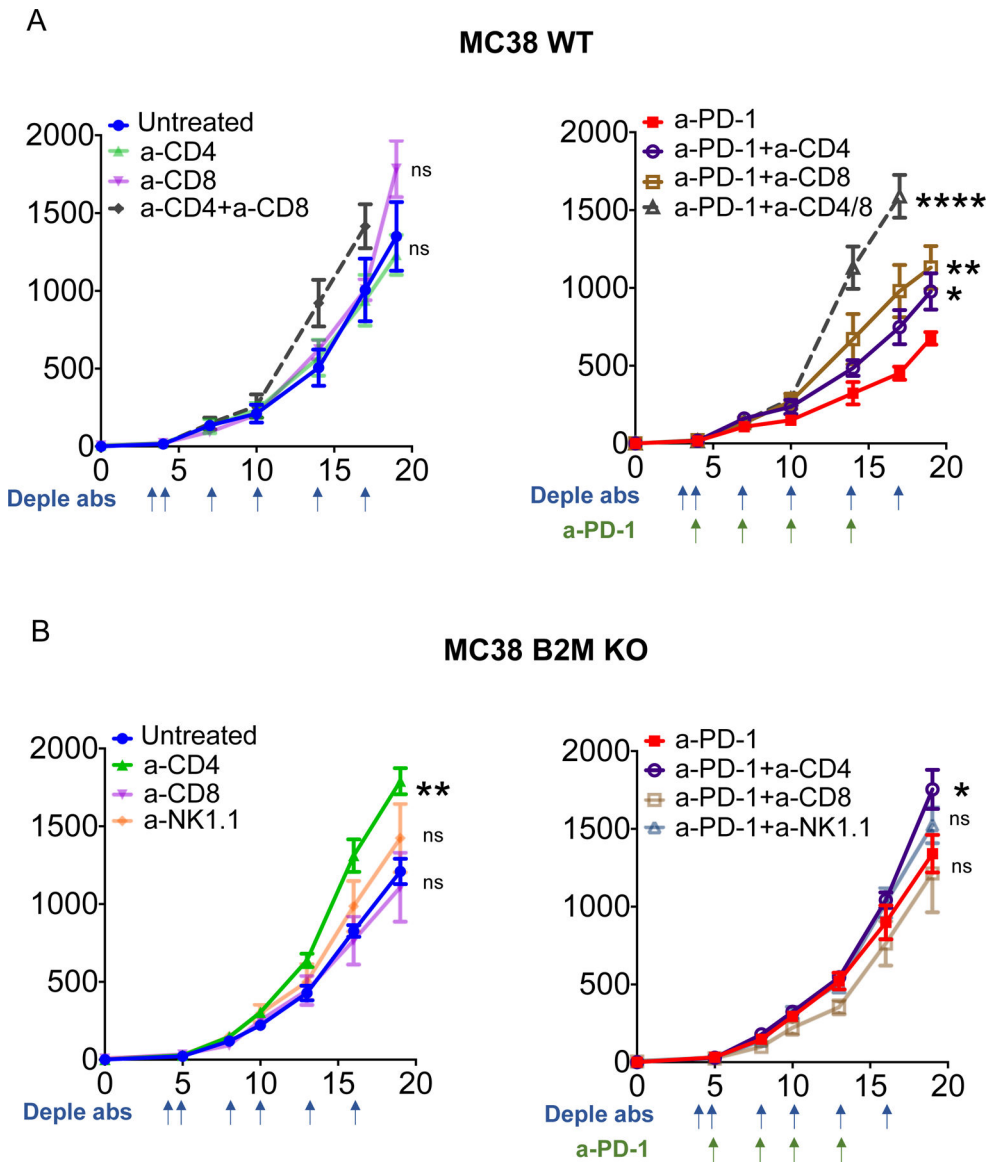

Figure 2. Immune cell subsets inducing antitumor responses in MC38 with and without *B2M* expression.

In vivo tumor growth curves of (A) wild-type (WT) and (B) *B2M*-knockout (KO) tumors of MC38. Data represented as mean ± SEM from an *n* of 5 per group. The arrow indicates the days of treatment with depletion antibodies or when anti–PD-1 was started. P values are shown for the last time point, ns, not significant; *, P < 0.05; **, P < 0.01; ****, P < 0.0001 versus untreated control, Unpaired *t* test. Data are representative of two or three independent experiments.

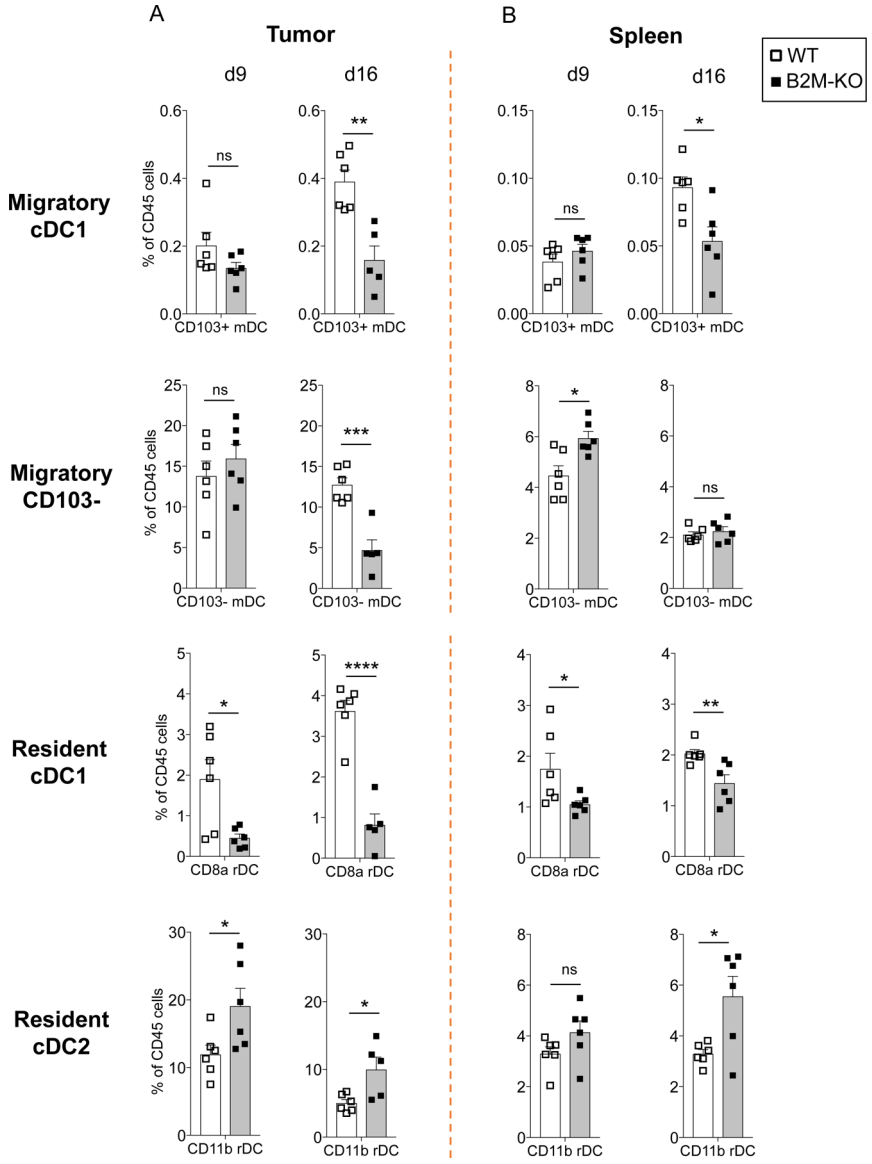

Figure 3. Dendritic cell subsets in MC38 with and without *B2M* expression.

Differences in the infiltration of CD103+ mDCs, CD103- mDCs, CD8+ rDCs and CD11b+ rDCs in MC38 WT and *B2M*-KO in (A) tumors and (B) spleens. Tumors were collected on day 9 (two doses of isotype or anti–PD-1) and day 16 (four doses of isotype or anti–PD-1). After processing and staining, samples were gated as indicated in Supplementary Figure 2. Mean ± SEM, Unpaired *t* test, $n = 6$. ns, not significant; *, $P < 0.05$; **, $P < 0.01$; ***, $P < 0.001$; ****, $P < 0.0001$.

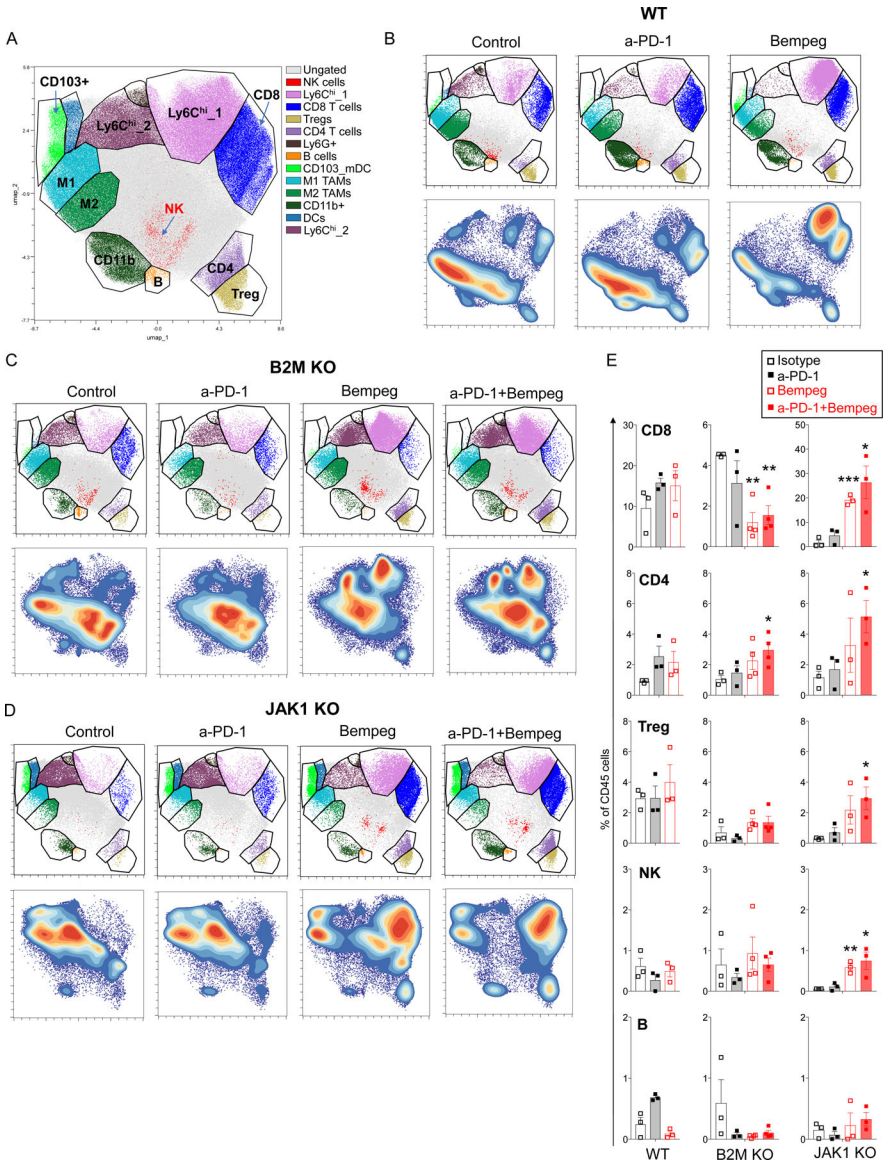

Figure 4. Characterization of the tumor immune infiltration by CyTOF using OMIQ platform.

Plots showing UMAP views providing comprehensive manually gated immune cell populations in (A) all samples (B) MC38 WT (C) MC38 *B2M*-KO and (D) MC38 *JAK1*-KO treated with isotype-control, anti–PD-1, bempegaldesleukin (bempeg) and anti–PD-1 plus bempeg. (E) Percentage of CD8+ T, CD4+ T, T regs, NK and B cells from CD45+ cells. Mean ± SEM, Unpaired *t* test, $n = 3–4$. *, $P < 0.05$; **, $P < 0.01$; ***, $P < 0.001$.

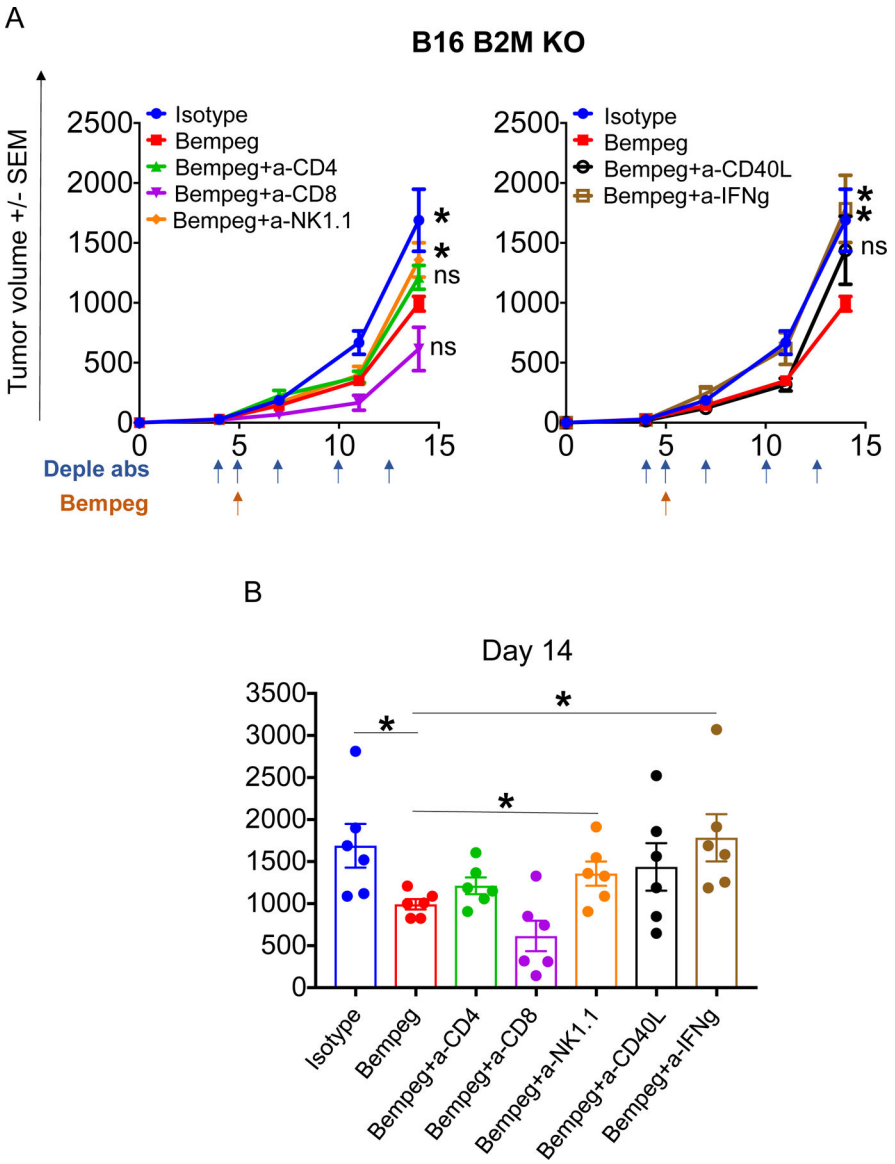

Figure 5. Immune cell subsets inducing antitumor responses in B16 with and without *B2M* expression.

(A) *In vivo* tumor growth curves and (B) tumor volumes at day 14 for B16 *B2M*-KO tumors with anti-CD4, anti-CD8, and anti-NK1.1, anti-CD40L and anti-IFNγ depletion studies after 0.8 mg/kg intravenous bempegaldesleukin. Data represented as mean ± SEM from an *n* of 6 per group. The arrow indicates the days of treatment with depletion antibodies or when bempegaldesleukin was started. Dunnett multiple comparisons test for bempegaldesleukin versus each condition: control, anti-CD4, anti-CD8, anti-NK1.1, anti-CD40L, anti-IFNγ. ns, not significant; *, $P < 0.05$. Data are representative of two independent experiments.

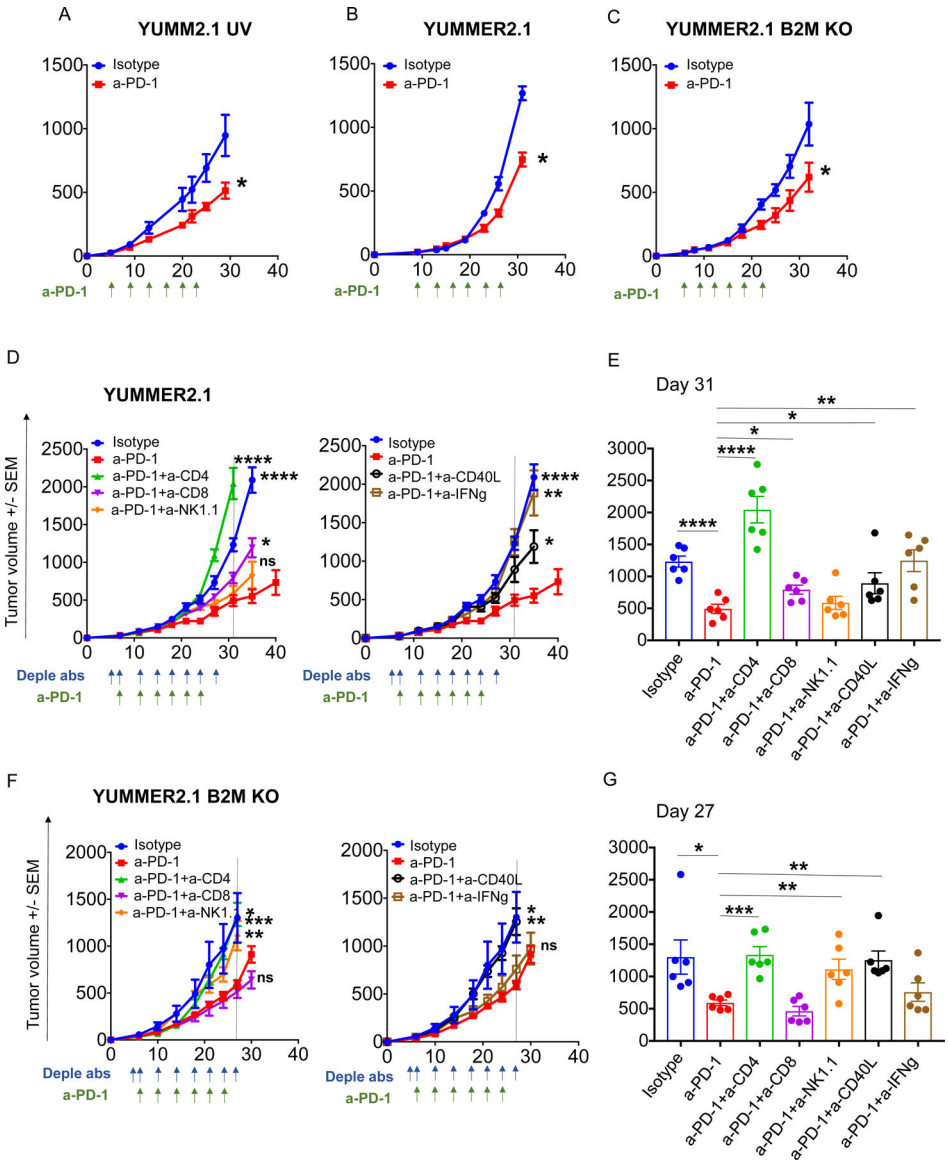

Figure 6. Immune cell subsets inducing antitumor responses in YUMMER2.1 with and without *B2M* expression.

In vivo tumor growth curves of (A) YUMM2.1 UV (B) YUMMER2.1 and (C) YUMMER2.1 *B2M*-KO tumors after isotype-control or anti-PD-1 therapy. In YUMM2.1 UV, $n = 4$ per group; YUMMER2.1, $n = 10$ per group and in YUMMER2.1 *B2M*-KO, $n = 5$ per group. In (A-C) the arrow indicates the days of anti–PD-1 treatment. *P* values are shown for the last time point; Unpaired *t* test; *, $P < 0.05$. Data are representative of two or three independent experiments. (D) In *vivo* tumor growth curves and (E) tumor volumes at day 31 for YUMMER2.1 with anti-CD4, anti-CD8, and anti-NK1.1, anti-CD40L and anti-IFNγ depletion after anti–PD-1 therapy. Data represented as mean ± SEM from an *n* of 6 per group. (F) In *vivo* tumor growth curves and (G) tumor volumes at day 27 for YUMMER2.1 *B2M*-KO with anti-CD4, anti-CD8, and anti-NK1.1, anti-CD40L and anti-IFNγ depletion after anti–PD-1 therapy. Data represented as mean ± SEM from an *n* of 6 per group. In (D) and (F) the arrow indicates the days of treatment with depletion antibodies

or when anti–PD-1 was started. Dunnett multiple comparisons test for anti–PD-1 versus each condition: control-isotype, anti-CD4, anti-CD8, anti-NK1.1, anti-CD40L, anti-IFNγ. ns, not significant; *, $P < 0.05$; **, $P < 0.01$; ***, $P < 0.001$; ****, $P < 0.0001$. Data are representative of two independent experiments.

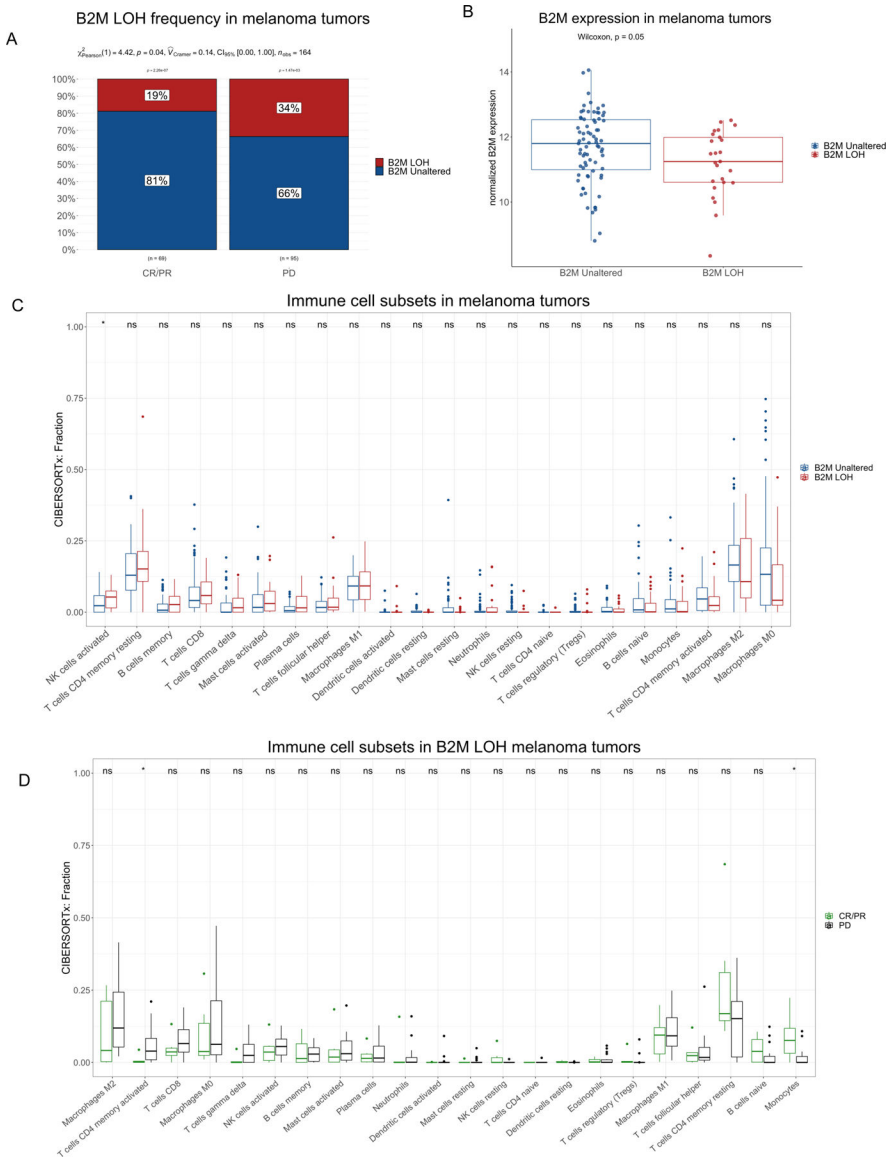

Figure 7. Baseline melanoma biopsies with and without *B2M* loss of heterozygosity (LOH).

(A) The frequency of LOH events in baseline responsive (n=69) versus progressive melanoma tumors (n=95); $X^2_{Pearson}$ test, p=0.04, n=164. (B) *B2M* expression levels in *B2M* unaltered (n=75) versus tumors with *B2M* LOH (n=25) determined using the normalized bulk RNAseq data (logcpm). Wilcoxon test, p=0.05, n=100. CIBERSORTx immune cell deconvolution analysis using bulk RNAseq data showing (C) fractions of immune cell types in *B2M* unaltered (n=75) versus *B2M* LOH tumors (n=25), and (D) fractions of immune cell subtypes in *B2M* LOH progressive (n=19) versus responsive tumors (n=6). Cell types are sorted by greatest difference in median score between groups. For the box and whisker plots, the central line represents the median, the upper line represents the upper quartile, the lower line represents the lower quartile, the point where the upper whisker ends represents the maximum, and the point where the lower whisker ends represents the minimum; all values

beyond the maximum and minimum represent outliers. Wilcoxon test, ns= not significant, * $P < 0.05$.